JOURNAL OF ENERGY SYSTEMS

2022, 6(2)

2602-2052 DOI: 10.30521/jes.1003175 Research Article

Step by step approach for developing analytical and experimental research facilities of a three-phase self-excited induction generator

Mohd Faisal Khan
Aligarh Muslim University, EES, University Polytechnic, F/O Engg. & Tech., Aligarh, India
mfaısal_khan@yahoo.com
Mohd Rizwan Khan
Aligarh Muslim University, Electrical Engineering Department, F/O Engg. & Tech., Aligarh, India
rizwan.eed@gmail.com

Submitted: 01.10.2021
Accepted: 19.03.2022
Published: 30.06.2022

Abstract: Self-excited induction generators (SEIGs) have been rigorously investigated in last few decades owing to their suitability for standalone renewable energy applications. Various issues pertaining to their modeling and control are quite aptly addressed in several analytical and experimental studies. However, these analyses are often focused on elaboration of proposed innovations and findings while the important details on modeling and implementation of SEIGs are left to be explored by readers. In this paper, a step by step approach for the mathematical modeling of three-phase self-voltage regulating, short shunt SEIG in stationary reference frame is explained. Subsequently, the developed d-q model of SEIG is implemented in terms of a simulation model. The developed model is then employed to carry out performance analysis of 3-phase, 2.2 kW SEIG supplying R-L load. All the results are verified with good accuracy in a SEIG test-rig whose details are included in the paper. The prime objective of this work is to provide a consolidated source for developing research resources of a self-voltage regulating three phase SEIG.

Keywords: *Dynamic modeling, Excitation capacitance, Experimental analysis, RL load, Series capacitance, Self-excited induction generator, Short shunt, Simulation*

Cite this paper as: Khan, M.F., & Khan, M.R., Step by step approach for developing analytical and experimental research facilities of a three-phase self-excited induction generator. *Journal of Energy Systems* 2022; *6*(2): 221-240, DOI: 10.30521/jes.1003175

Nomenclature	
R_s,R_r, R_L	stator, rotor and load resistances (ohms)
L_{sl},L_{rl}	stator & rotor leakage inductances (Henry)
Ψ_{sd}, Ψ_{sq}	d and q axes stator flux(Wb)
Ψ_{rd}, Ψ_{rq}	d and q axes rotor flux(Wb)
Ψ_{rd0}, Ψ_{rq0}	d and q axes initial rotor flux(Wb)
v_{dcap}, v_{qcap}	d and q axes instantaneous voltages across excitation capacitance (volts).
v_{dcse}, v_{qcse}	d and q axes instantaneous voltages across series capacitance (volts).
V^0_{qcap} , V^0_{dcap}	d and q axes voltages due to initial charge on excitation capacitance(volts)
v^0_{rq},v^0_{rd}	d and q axes rotor induced voltages due to remnant flux(volts)
V_T	terminal voltage(volts)
V_L	load voltage (volts)
L_m	magnetizing inductance (Henry)
L_L	load inductance (Henry)
I_L	load Current(amps)
P_o	active power generated (watts)
C_{ex}	shunt or excitation capacitance(μF)
C_{se}	series or compensation capacitance(μF)
Ψ_m	magnetizing flux (Wb)
T_e	Electromagnetic Torque (Nm)
i_{dcap}, i_{qcap}	d and q axes capacitor currents(amps)
i_{sd}, i_{sq}	d and q axes stator currents(amps)
i_{rd}, i_{rq}	d and q axes rotor currents(amps)
i_{Ld}, i_{Lq}	d and q axes load currents(amps)
I_s	stator current(amps)
I_m	magnetizing current(amps)
I_c	excitation capacitor current(amps)
ω_r	rotor electrical speed(rads/sec)

1. INTRODUCTION

Three phase self-excited induction generators (SEIGs) are the most implemented variant of SEIGs due to the universally accepted poly-phase transmission systems. Therefore, an exhaustive body of research on three-phase SEIGs exists in the literature dealing with different modeling [1-5], control [6-11] and operational approaches [12-19]. However, due to the specific nature of these studies step by step mathematical modeling and the simulation as well as experimental implementation of SEIG are not considered simultaneously. The present work renders complete details regarding dynamic modeling, Simulink model development and the test-rig preparation of a three-phase self-voltage regulating SEIG.

Large scale area of the application of three-phase SEIGs is found to be in wind electric power generation systems although they may also be deployed in mini/micro hydro generation systems [20]. Owing to their squirrel caged construction, they come across as extremely rugged and fault tolerant machines offering excellent durability [19] which is the foremost requirement in their fields of application. Capacitor excited and compensated SEIGs are attractive preposition as standalone generating units for supplying off-grid loads [2,22]. Thus, due to their popularity and penetration in renewable generation systems, various approaches for the modeling of three-phase SEIGs have been implemented successfully in the literature by a number of studies.

Seyoum et al [1] have developed *d-q* model of a three-phase SEIG in stationary reference frame to highlight the effects of magnetizing inductance, L_m on the SEIG performance. The ability of L_m to stabilize the terminal voltage after transient states such as self-excitation, loading, un-loading and the change in input speed is given an in-depth treatment. The synchronous reference frame model developed by Palle et al [2] is utilized to study the transients caused by differences in instantaneous voltage and frequencies of multiple SEIGs connected in parallel. A novel method of constant stator current and load voltage operation for a three phase SEIG is proposed by Haque in Ref. [3] through steady state model optimized by the Matlab tool fsolve for the calculation of unknowns i.e. frequency and the magnetizing reactance. Bašic et. al [4] have proposed a novel dynamic model of SEIG in stationary reference frame that incorporates the iron losses represented by an iron loss resistance connected in parallel with the stator inductance. Initiation of self-excitation under different preconditions and the ability of a three-phase SEIG to ride through transient change in input speed are considered for the analysis by Khan and Khan in [5] based on dynamic modeling approach in stationary reference frame.

Inherently poor voltage and frequency regulations of SEIGs entail implementation of suitable corrective measures [23,24]. Although frequency control is not considered in the present analysis, the voltage control mechanism is devised with the selection of a suitable self-voltage regulating scheme. Numerous voltage regulating schemes have been developed and integrated with the SEIGs could be referred from [6-9] and [25-30].

The Artificial Intelligence (AI) based controllers [25-27] have not found much favour with SEIGs due to complexities involved [1]. Similarly, the microcontroller based voltage regulators [20] have been discouraged due to their costly nature. The reactive power regulation of SEIGs through power electronic based schemes such as switched capacitors [9], SVCs [28], STATCOMs [7] and the DSTATCOMs [8] induce harmonics thereby affecting the power quality and are prone to frequent breakdowns.

Non-power electronic based voltage controllers such as saturable core reactors and constant voltage transformers are bulky and hence may not be suitable for standalone applications [29]. Series compensation through a carefully selected optimum series capacitance has yielded good results for SEIG applications [29]. The scheme is simple, cost effective and does not use power electronic switches and hence supports the ruggedness of SEIG. For this study series capacitance based short shunt scheme [21,22] is considered for the self-voltage regulation.

Present work deals with the development of step by step dynamic model of a three-phase short shunt SEIG in stationary reference frame. The derived mathematical model is then implemented in terms of simulation model on Simulink platform. Details of various block sets of the developed simulation model are included for a better and clear understanding of the model. Further on, various technical issues and requirements for the preparation of three-phase SEIG test rig are explained in detail. The developed simulation model is then employed to extract the performance characteristics of the studied SEIG supplying *R-L* load along with the verification of results on developed test rig. Selection of series capacitance is given detailed treatment through experimental results demonstrating effects of capacitance variation on load voltage. The paper is written with the intention to provide a consolidated literature that renders all the necessary details for the up-coming researchers in this field.

From the available literature on SEIGs, as discussed above, it is clear that no consolidated work has thus far been put forth to present mathematical modeling, experimental implementation and related details to develop resources for SEIG analysis. This work endeavors to put together all these details to act as ready reference and assist the upcoming researchers in the realm of SEIGs. Main objectives and contributions of the study are mentioned as follows: The objectives are to develop a consolidated document for developing SEIG research facility, to implement a simple and user friendly voltage regulating scheme for SEIGs, to analyze SEIG performance with different power factor loads and to present details on setting up a working test rig of SEIG. The contributions are detailed mathematical modeling and simulation of a three-phase short shunt SEIG with the help of necessary block diagrams, developed SEIG model for resistive-inductive loading and experimental validation in a test-rig with 2.2 kW.

The paper consists of six sections: Section 1 provides an introduction and summarizes proposed study. Section 2 deals with mathematical modeling of short shunt SEIG. Section 3 puts forth the details of simulation model. Section 4 renders all the details regarding test-rig and its working. Section 5 provides detailed discussion on simulation and experimental results of developed SEIG supplying *R-L* load. Section 6 provides main conclusions of the study.

2. MODELING OF SHORT SHUNT SEIG

The *d-q* model of a three phase short shunt SEIG incorporating various flux linkages is depicted in Fig. 1, while Fig. 2 illustrates block diagram of overall implementation of scheme. The model is derived from the fundamental model of a three phase induction machine with necessary modifications for generation mode of operation. By switching *S1* and *S2* "ON" and "OFF" appropriately various operating conditions such as no-load, on load with and without series compensation can be easily simulated.

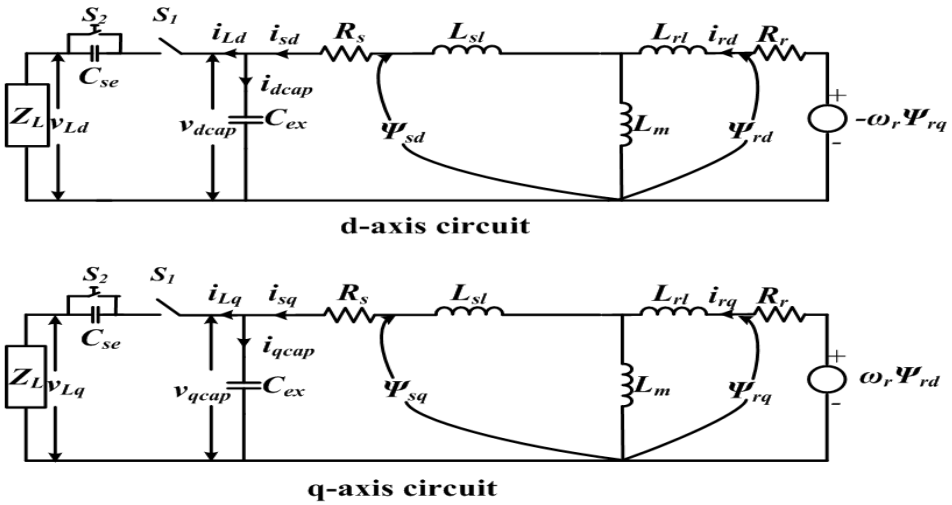

Figure 1. d-q model of a three phase SEIG.

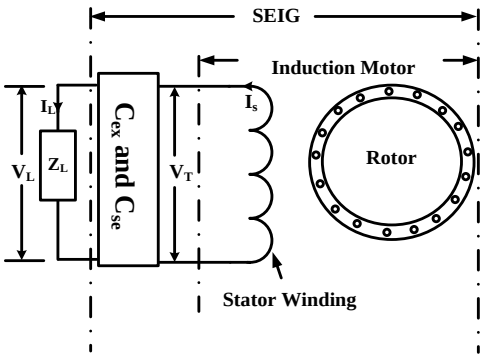

Figure 2. Description of SEIG scheme using an induction machine implemented for the analysis.

From the differential equations of three phase SEIG defining the flux linkages between various passive elements, the machine model may be represented by the state space equation given by Eq. 1 [1,21, 22, 31].

$$p\begin{bmatrix} i_{sq} \\ i_{sd} \\ i_{rq} \\ i_{rd} \end{bmatrix} = -\frac{1}{L_m^2 - L_s L_r}\left(\begin{bmatrix} -L_r R_s & -L_m^2\omega_r & L_m R_r & -L_m\omega_r L_r \\ L_m^2\omega_r & -L_s R_s & L_m\omega_r L_r & L_m R_r \\ L_m R_s & L_m\omega_r L_s & -L_s R_r & -L_r\omega_r L_s \\ -L_m\omega_r L_s & L_m R_s & -L_r\omega_r L_s & -L_s R_r \end{bmatrix} \begin{bmatrix} i_{sq} \\ i_{sd} \\ i_{rq} \\ i_{rd} \end{bmatrix} + \begin{bmatrix} -L_r & 0 & L_m & 0 \\ 0 & -L_r & 0 & L_m \\ L_m & 0 & -L_s & 0 \\ 0 & L_m & 0 & -L_s \end{bmatrix} \begin{bmatrix} v_{qcap} \\ v_{dcap} \\ v_{rq}^0 \\ v_{rd}^0 \end{bmatrix} \right) \quad (1)$$

From Eq. 1 the SEIG currents may be expressed as,

$$pi_{sq} = \frac{1}{L_r L_s - L_m^2}\left(-L_r R_s i_{sq} - L_m^2\omega_r i_{sd} + L_m R_r i_{rq} - L_m\omega_r L_r i_{rd} - L_r v_{qcap} - L_m v_{rq}^0\right) \quad (2)$$

$$pi_{sd} = \frac{1}{L_r L_s - L_m^2}\left(L_m^2\omega_r i_{sq} - L_s R_s i_{sd} + L_m\omega_r L_r i_{rq} + L_m R_r i_{rd} - L_r v_{dcap} + L_m v_{rd}^0\right) \quad (3)$$

$$pi_{rq} = \frac{1}{L_r L_s - L_m^2}\left(L_m R_s i_{sq} + L_m\omega_r L_s i_{sd} - L_s R_r i_{rq} + L_s L_r\omega_r i_{rd} + L_m v_{qcap} + L_s v_{rq}^0\right) \quad (4)$$

$$pi_{rd} = \frac{1}{L_r L_s - L_m^2}\left(-L_r L_m\omega_r i_{sq} + L_m R_s i_{sd} - L_s\omega_r L_r i_{rq} - L_s R_r i_{rd} + L_m v_{dcap} - L_s v_{rd}^0\right) \quad (5)$$

Following Eqs. 2 to 4, some of the variables represent machine parameters and may be calculated from the standard tests available for the same [32]. However, besides the standard machine parameters the magnetizing inductance L_m (which is dynamic for generator operation) and the stator and rotor induced voltages have to be found for the solution. In the above equations ω_r represents the electrical speed of the rotor and may be expressed as, $\omega_r=(P_N/2)$ x *mechanical input speed*. Here P_N is the number of poles. When the rotor electrical speed combines with the q and d rotor fluxes the rotor induced speed voltages along the same axes may be expressed as [1,21,22,31]:

$$\left.\begin{aligned} \omega_r\psi_{rq} &= \omega_r\left(L_m i_{sq} + L_r i_{rq}\right) + v_{rd}^0 \\ \omega_r\psi_{rd} &= \omega_r\left(L_m i_{sd} + L_r i_{rd}\right) + v_{rq}^0 \end{aligned}\right\} \quad (6)$$

The modeling of different SEIG parameters defining the no-load and on-load dynamics of the machine is further taken-up as follows:

Modeling of excitation capacitance:

$$v_{qcap} = \frac{1}{C_{ex}} \int i_{qcap} dt + V_{qcap}^{0} \quad (7)$$

$$v_{dcap} = \frac{1}{C_{ex}} \int i_{dcap} dt + V_{dcap}^{0} \quad (8)$$

Here, $i_{dcap}=i_{sd}$ and $i_{qcap}=i_{sq}$

Modeling of series capacitance:

$$v_{qcse} = \frac{1}{C_{se}} \int i_{Lq}\ dt \quad (9)$$

$$v_{qcse} = \frac{1}{C_{se}} \int i_{Lq}\ dt \quad (10)$$

Modeling of load:

$$pi_{Lq} = \frac{v_{qcap}}{L_L} - \frac{R_L}{L_L} i_{Lq} - \frac{1}{L_L C_{se}} \int i_{Lq} dt \quad (11)$$

$$pi_{Ld} = \frac{v_{dcap}}{L_L} - \frac{R_L}{L_L} i_{Ld} - \frac{1}{L_L C_{se}} \int i_{Ld} dt \quad (12)$$

Now, $i_{dcap}=i_{sd}-i_{Ld}$ and $i_{qcap}=i_{sq}-i_{Lq}$, thus,

$$v_{qcap} = \frac{1}{C_{ex}} \int (i_{sq} - i_{Lq}) dt + V_{qcap}^{0} \quad (13)$$

$$v_{dcap} = \frac{1}{C_{ex}} \int (i_{sd} - i_{Ld}) dt + V_{dcap}^{0} \quad (14)$$

$$v_{Lq} = v_{qcap} - v_{qcse} \quad (15)$$

$$v_{Ld} = v_{dcap} - v_{dcse} \quad (16)$$

Calculation of quantities:

RMS currents:

$$I_{rms} = \sqrt{\frac{i_q^2 + i_d^2}{2}} \quad (17)$$

RMS voltages:

$$V_{rms} = \sqrt{\frac{v_q^2 + v_d^2}{2}} \quad (18)$$

Torque and generated power:

$$P_o = \frac{3}{2}\left(v_q i_q + v_d i_d\right) \quad (19)$$

$$T_e = 0.75 P_N L_m \left(i_{sd} i_{rq} - i_{sd} i_{rd}\right) \quad (20)$$

2.1. Significance of v_{rq}^0,v_{rd}^0 ,V_{qcap}^0 *and* V_{dcap}^0 for Initiation of Self-Excitation

The mechanism of voltage build-up in a SEIG is similar to that of a self excited dc generator. The initial voltage in a SEIG, however, can be derived either from the rotor core or the excitation capacitances. This initial or residual voltage causes transient magnetizing currents to flow in the stator windings thereby charging the capacitances which in turn further increase this current and so on. A detailed analysis of voltage build-up in a SEIG with different modes of excitations is explained by Khan and Khan in [5].

As the residual voltages of rotor core or excitation capacitances play central role in self-excitation and voltage build-up in SEIG they have to be appropriately represented in the mathematical model. Thus, the quantities v_{rq}^0 andv_{rd}^0 respectively represent initial voltages along q and d axes in the rotor core. Likewise, the initial voltage due to remnant charge in the excitation capacitances is represented by V_{qcap}^0 *and* V_{dcap}^0 along the *q* and *d* axes respectively. For an accurate matching of simulation and the experimental results these voltages have to be taken as equal. Initial voltage due to remnant flux in the core can be easily measured at the stator terminals using a multi-meter with excitation capacitances disconnected. Similarly, the initial voltage in capacitances can be recorded with the same multi-meter across their connecting leads of excitation capacitances.

2.2. Evaluation of Magnetizing Characteristic

In order to ensure that the SEIGs operate in the saturation region of the magnetizing characteristic for a given machine the magnetizing inductance, L_m plays a crucial role. By ensuring saturated operation of induction machine operating as SEIG the magnetizing inductance maintains steady state across various operating points. Therefore, the magnetizing inductance for a SEIG is dynamic in nature unlike motoring application wherein the supply voltage is fixed. It is therefore paramount for any analytical model of SEIG that variation of L_m with the voltage is accurately estimated so that it is utilized to get precise results. In this paper the characteristic defining relationship between magnetizing inductance and the per phase voltage is extracted through synchronous speed test [33]. The test is performed on the open stator winding induction machine utilized for poly-phase SEIG operation. Detailed procedure for performing the test is given in *Appendix*.

The data yielded by the test is plotted to obtain the magnetizing characteristic of machine formulated in terms of Eq. 21 yielded by the 3rd order curve fitting of test data.

$$L_m = -5.3635e^{-009} V_{ph}^3 - 1.8533e^{-007} V_{ph}^2 + 0.0029168\, V_{ph} + 1.1034 \qquad (21)$$

3. SIMULINK MODEL OF SHORT SHUNT SEIG

Block schematic of developed simulink model of the SEIG is shown in Fig. 3. In order to gain an in-depth understanding on various sub-blocks of the model, brief description of each of the main block is included in subsequent sections.

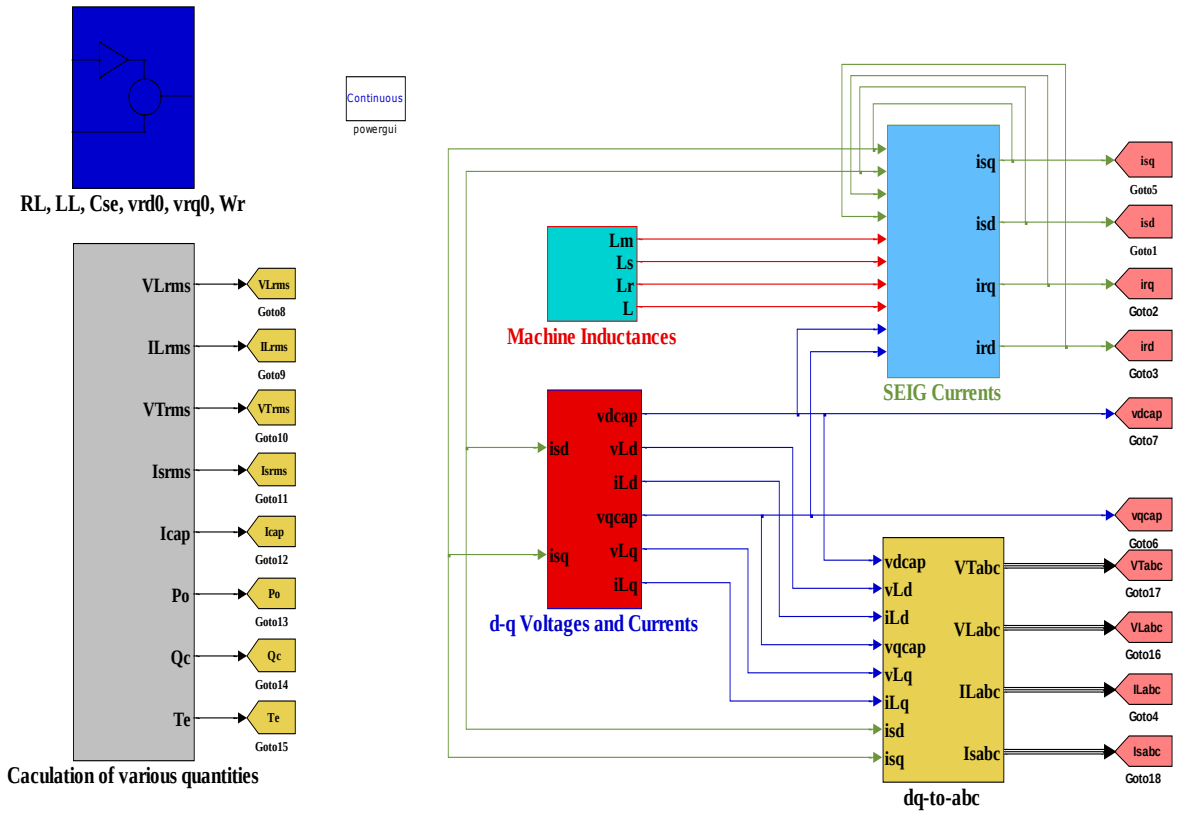

Figure 3. Simulink model of three phase SEIG

3.1 Explanation of Major Sub-blocks

Depiction of various sub-blocks of Simulink model of studied SEIG and brie explanation of each is presented below.

3.1.1 D-Q axis capacitor voltage simulation blocks

The *d-q* voltages across capacitor are evaluated by implementing Eqs. 13 and 14 described in SEIG model derived in Section 2. Details of the blocks are depicted in Figs. 4(a,b). As can be seen in both the block diagrams, the load current i_L is obtained from the output of integrator 2 block. This current is afterwards used to calculate load *d-q* load voltages from Eqs. 15 and 16.

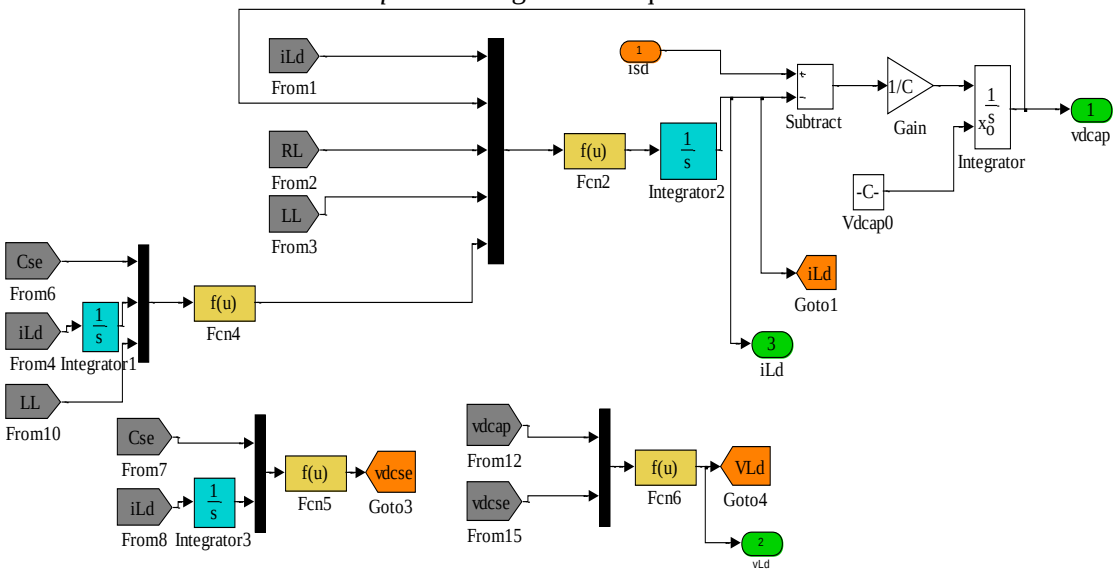

(a)

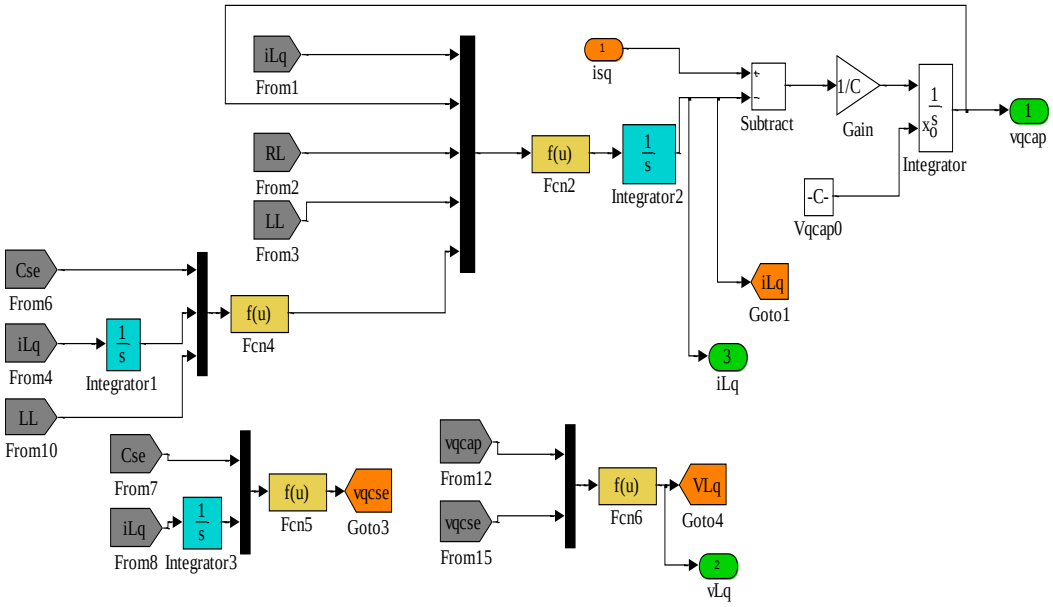

(b)

Figure 4. d-q Axis Capacitor voltage blocks of the developed SEIG model: (a) d-axis capacitor voltage simulation (b) d-Axis capacitor voltage simulation.

3.1.2 SEIG inductance calculation blocks

Blocks for calculating the inductances and associated quantities of SEIG are depicted in Figs. 5(a-d). The magnetizing inductance L_m is calculated in accordance with Eq. 21 for different voltages induced at the SEIG terminals. Thus, as can be seen from Fig. 5(a) for a given value of input voltage V_{srms}, the block yields L_m which is used for simulation. The magnetizing current I_m is calculated from the block depicted in Fig. 5(b). Stator and rotor inductances L_s and L_r can be calculated as illustrated in Fig. 5(c) while the inductance $L=L_rL_s-L_m^2$ from Fig. 5(d).

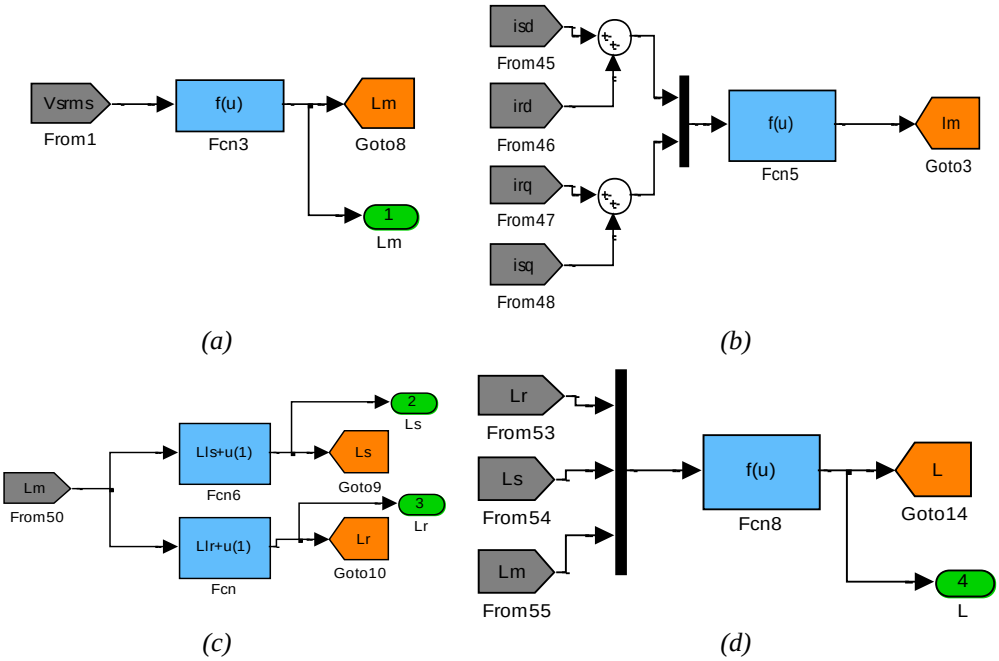

(a) *(b)*

(c) *(d)*

Figure 5. Blocks for calculation of various inductances of studied SEIG. (a) Calculation block of L_m, (b) Calculation block of i_m, (c) Calculation block of stator and rotor inductances L_s and L_r, (d) Calculation block of L.

3.1.3 Calculation of RMS values of parameters

For the calculation of magnitudes of different output parameters of SEIG, the simulink blocks depicted in Figs. 6(a-d) are put together. The rms value of stator voltage/current and load voltage /current is obtained by the simulink blocks illustrated respectively in Fig. 6(a) and Fig. 6(b). While the electromagnetic torque and generated output power is obtained from Fig. 6(c) and Fig. 6(d).

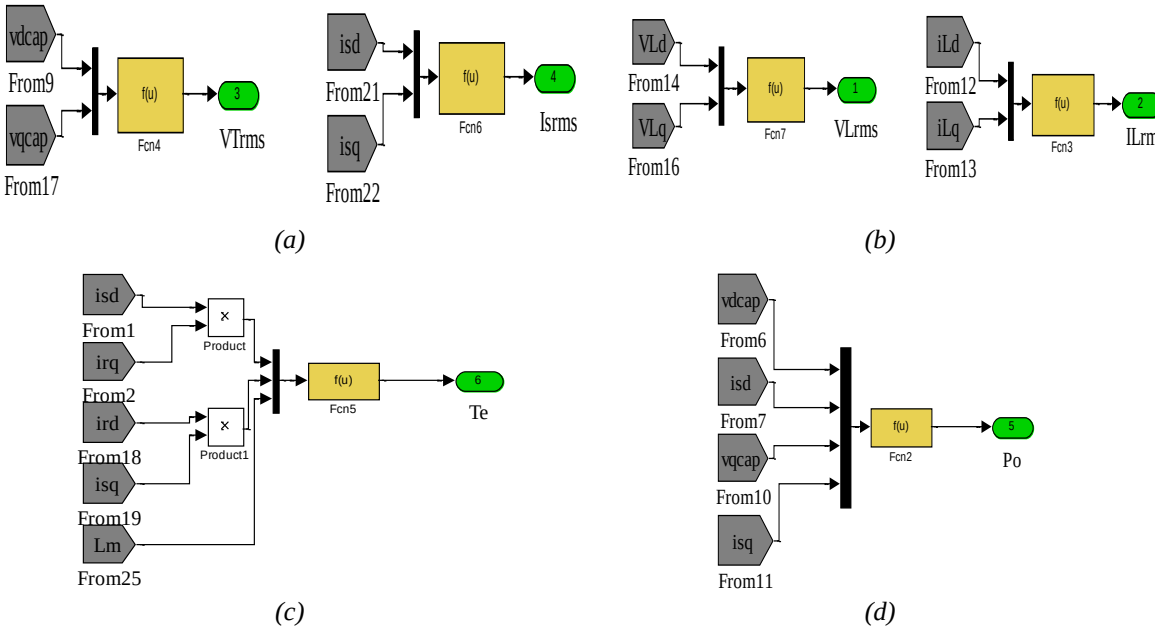

Figure 6. RMS value calculation blocks for (a) stator voltage and current (b) load voltage and current (c) electromagnetic torque (d) generated output power.

4. DESCRIPTION OF EXPERIMENTAL SETUP

Test-rig arrangement and details of associated equipments are illustrated in Fig. 7. An open end winding (OeW), squirrel caged induction machine is employed for operation as a SEIG. The excitation capacitances are accommodated as a *Y* connected bank. A 3ph, 3.7 kW induction motor is employed as prime mover. Then prime mover speed is regulated by means of an AC inverter drive. .

4.1. General Construction Details of OeW Induction Machine

The OeW machine is wound with double layer windings. The features are with conductors/slot=150=75x2; SWG=22, wt/coil=125 grms; slots=36, coils=36, double layer winding; Pitch=6. Two ends of each coil are marked as B for (Bottom placed) and T for (Top placed) for identification. Thus total terminals available on the panel are 72 marked as (1-36)B and (1-36)T. For three-phase, star connection of the machine 9 coils/phase are dedicated. The OeW machine offers advantage of having flexibility of getting different configurations of connection such as star and delta. The choice of OeW machine for this study is purely made on the basis of convenience and availability. Therefore, any general purpose off the shelf squirrel cage type induction machine may be utilized.

Figure 7. Illustration of three-phase short shunt SEIG test rig.

4.2 Rating and Specifications of Equipments used

SEIG: 400 V, 3 hp/2.2 kW, 4.5 A, OeW squirrel caged induction machine.
Per phase winding parameters of SEIG: R_s=12.6 Ω, R'_r=15.1 Ω, L_{ls}=L_{lr}=0.0640 H.
Prime Mover: 3-phase, Delta connected, 415 V, 7.6 A, 3.7 kW, 1430 rpm, 50 Hz, Squirrel caged induction motor.
Loading Rheostat: 3 panels each of 3 phase, 1.5 KW, 415 V rating.
Inductive Load: 3 X 180 mH, (steps:12,24,30,60,90,120,180mH).
Speed Controller: YASKAWA, VARISPEED, 616G5, Inverter Drive, 3 phase, 400 V, 2.2 kW.
DSO: Tektronix TPS 2024, 4 channel Digital Storage oscilloscope, 200 MHz, 2GS/s

5. PERFORMANCE ANALYSIS

The developed simulation and experimental facilities are utilized for the extraction of performance characteristics of SEIG. The SEIG analysis is done for the rated loads of unity and 0.9 lagging power factors to establish optimality of developed model and verify it on the test-rig. The detailed results and their interpretations are presented in the following sections. For the entire analysis, unless mentioned in a specific context, the SEIG is driven by regulated prime mover at 1500 rpm i.e., the rated value maintained by means of speed controller.

5.1. Selection of Excitation and Compensation Capacitances

For standalone operation the reactive power of SEIG is to be supplied by terminal capacitances connected across their stator windings, hence, the foremost task to be fulfilled is the selection of optimum excitation capacitances. A number of procedures and algorithms for the selection of optimum excitation capacitances are available in the literature [1,3,12,34]. In this analysis the optimum excitation capacitance is selected experimentally utilizing the test-rig. An optimum excitation capacitance for SEIGs is defined to be the one which is able to establish rated no-load voltage across SEIG terminals at the rated input speed [35].

5.1.1. Selection of optimum excitation capacitance

For the investigated machine an excitation capacitance of 15 μF/phase is found to be optimum as it sets up 230 V at 1500 rpm across the terminals of SEIG as shown in Fig. 8. The configuration (i.e., star or delta) in which three phase excitation capacitance bank is connected to the stator windings does not make any difference so long as per phase optimum excitation capacitance corresponds to optimum value. However, if the star connection is to be implemented then each capacitance in the bank must be 3 times the per phase optimum value.

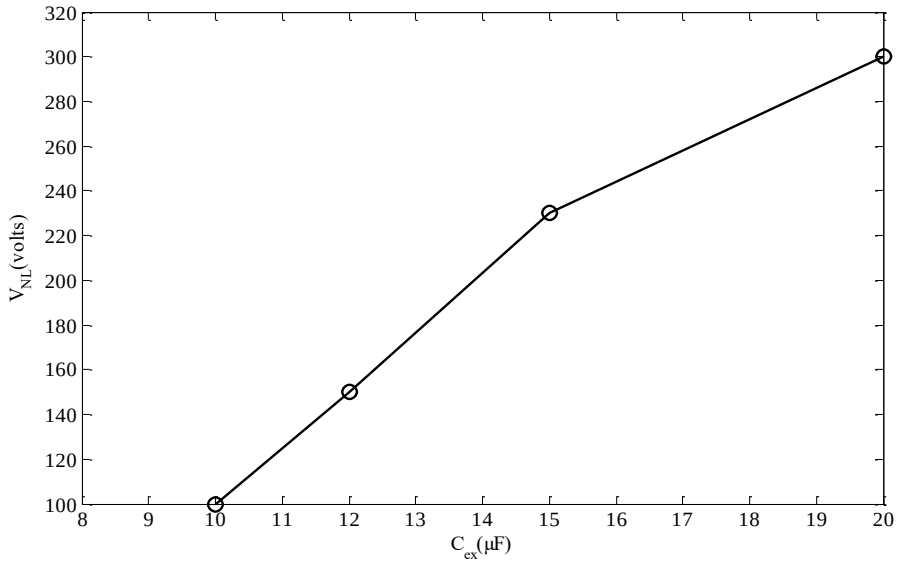

Figure 8. Variation of no-load voltage of SEIG with per phase excitation capacitance at rated speed of 1500 rpm.

In the present case the capacitance bank is connected in star to maintain consistency with the stator winding connection of SEIG, thus each capacitance of the bank is 45 μF. An analysis of the characteristic of Fig. 5 reveals that the SEIG is more sensitive to the variation in excitation capacitance values on the decreasing side. It can be seen that as the excitation capacitance is reduced by 33% of the optimum value to 10 μF the corresponding no-load generated voltage of SEIG decreases by 44% of rated no-load value to 100 V. In contrast, when the excitation capacitance is increased by the same factor of 33% to 20 μF the generated voltage increases to 300 V (rms) i.e. by about 30%. To record these results the excitation capacitances are connected to the SEIG terminals and then its speed is increased gradually through the prime mover up to rated value of 1500 rpm. The generated voltage has to be monitored continuously so as not to let it increase too much beyond the safe limits. Alternately, the voltage build-up could also be achieved by first bringing the SEIG up-to rated speed and then connecting the capacitance bank to its terminals through a switch. However, such a strategy may result in dangerously high generated voltage across SEIG terminals if the excitation capacitance is too high for the rated speed. It is also observedthrough the analysis that an excitation capacitance less than 8 μF fails to induce any self-excitation and hence no-voltage build-up occurs.

The inherent inability of SEIGs to supply practical loads is demonstrated from the simulated and recorded results of Fig. 9. Here, as soon as the full load of 2.2 kW at unity pf is switched on to the SEIG terminals the voltage immediately collapses to zero. This is due to the inability on the part of excitation capacitances to feed enhanced reactive power of SEIG on account of connected load resulting in the voltage collapse. Therefore, in order to make them practically viable for supplying the required loads, SEIGs have to be equipped with suitable voltage compensation devices.

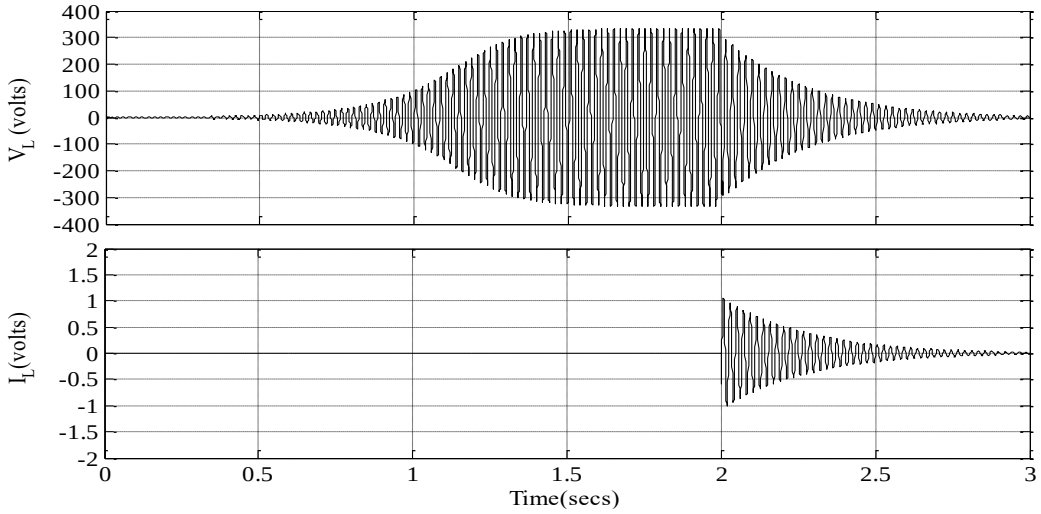

(a)

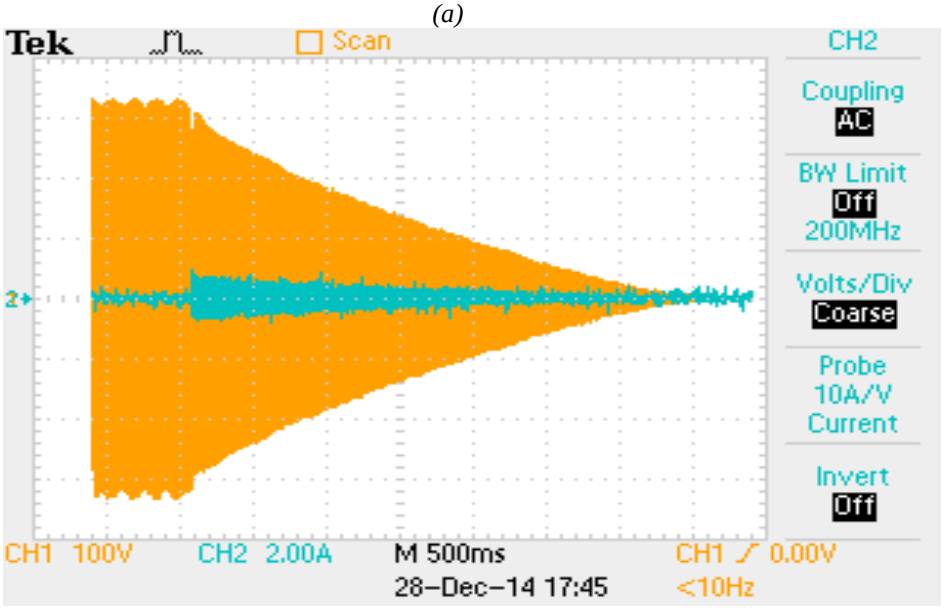

(b)

Figure 9. Voltage collapse on application of full load to three phase SEIG terminals operating without series capacitance (a) simulated (b) recorded

5.1.2. Selection of optimum series (compensation) capacitance

There can be a number of configurations for connecting series capacitances for the reactive power compensation of load such as long shunt, short shunt or a combination of two [21,29]. The long shunt or the combined scheme suffers from the drawback of excessive voltage drop across the series capacitances as they are placed in stator circuit of SEIG in former and both in stator and load circuits in the later. Due to this, although these schemes are able to achieve good voltage regulation the generated voltage is required to be stepped up as less voltage appears across the terminals over the entire range from no-load to full load due to high drop. However, in the short shunt mode the series capacitances are placed in load circuit and hence only load current passes through them. Thus, the value of series capacitances is much lower as compared to long shunt connection [21,29].

External characteristics of SEIG operated without any compensation and with short shunt compensation connection supplying unity power factor load are depicted in Fig. 10. When no series compensation is facilitated the SEIG output voltage profile is expectedly poor. The gross output power generated by SEIG under this mode of operation is 590 W that is about 26 % of the machine rating at a poor voltage regulation of 20 %.

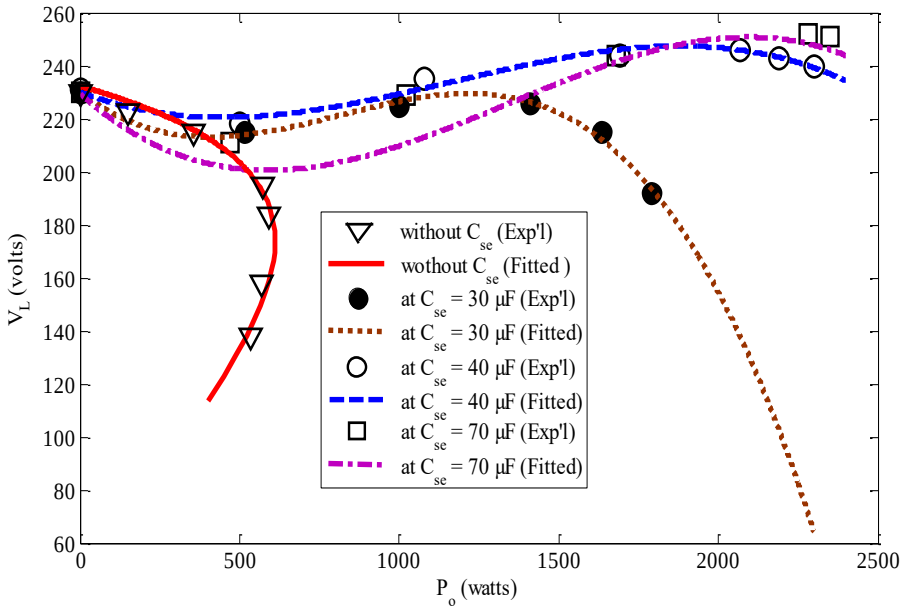

Figure 10. Measured external characteristics of three phase SEIG without series capacitance and with different series capacitances.

For self-compensated mode of operation each of the three phases of SEIG are equipped with series capacitances of 30 µF, 40 µF, 50 µF, and 70 µF denominations one by one in short shunt configuration. It is evident from Fig. 7 that 40 µF capacitance enables the SEIG to maintain most optimum performance. The series capacitance is able to maintain load voltage within ± 6.9 % of the no-load voltage over the entire output power range and a full load voltage regulation of -3.9% which is quite acceptable. Whereas, the corresponding range for 50 µF, and 70 µF series capacitances is -10 % and -12 % respectively. It is also observed that only 30 µF series capacitance is unable to meet rated power demand. From this analysis it is found that a capacitance of 40 µF in series with each phase yields best load voltage profile.

The load voltage, current, active and reactive powers along with the pf and the voltage harmonics for each of the series capacitances supplying up-to rated load of unity pf are recorded on a DSO. The recorded results are depicted from Figs. 11-14 while those at optimum series capacitances i.e. 40 µF are also obtained through simulation model. The simulated and recorded result parameters are found to be converging quite satisfactorily within a tolerance of ±3%.

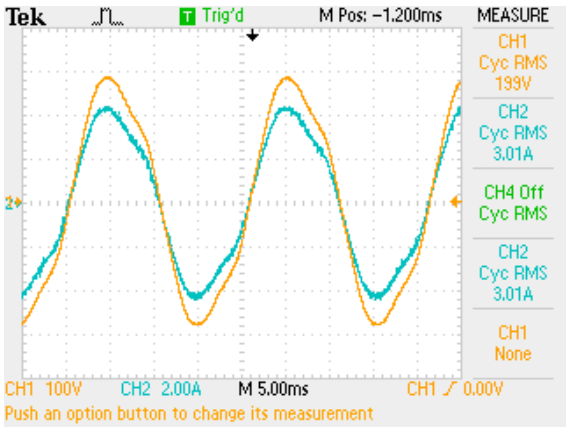

(a)

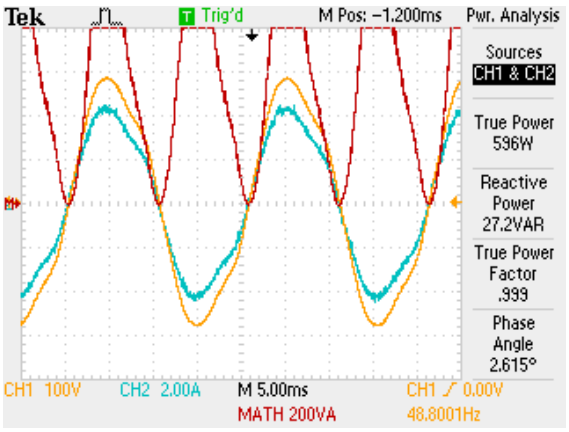

(b)

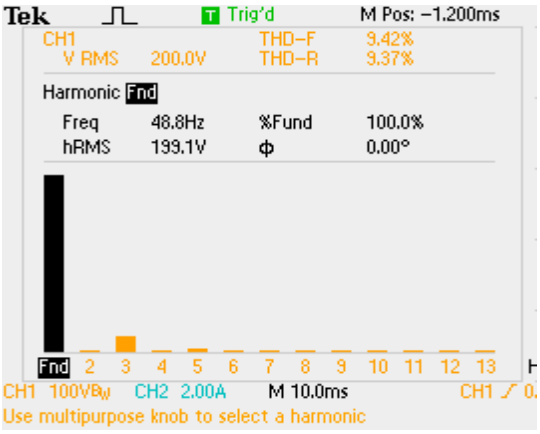

(c)

Figure 11. Recorded parameters of phase A at series capacitance of 30 µF at unity pf (a) load voltage and current (b) true and reactive powers along with operational pf (c) load voltage harmonics.

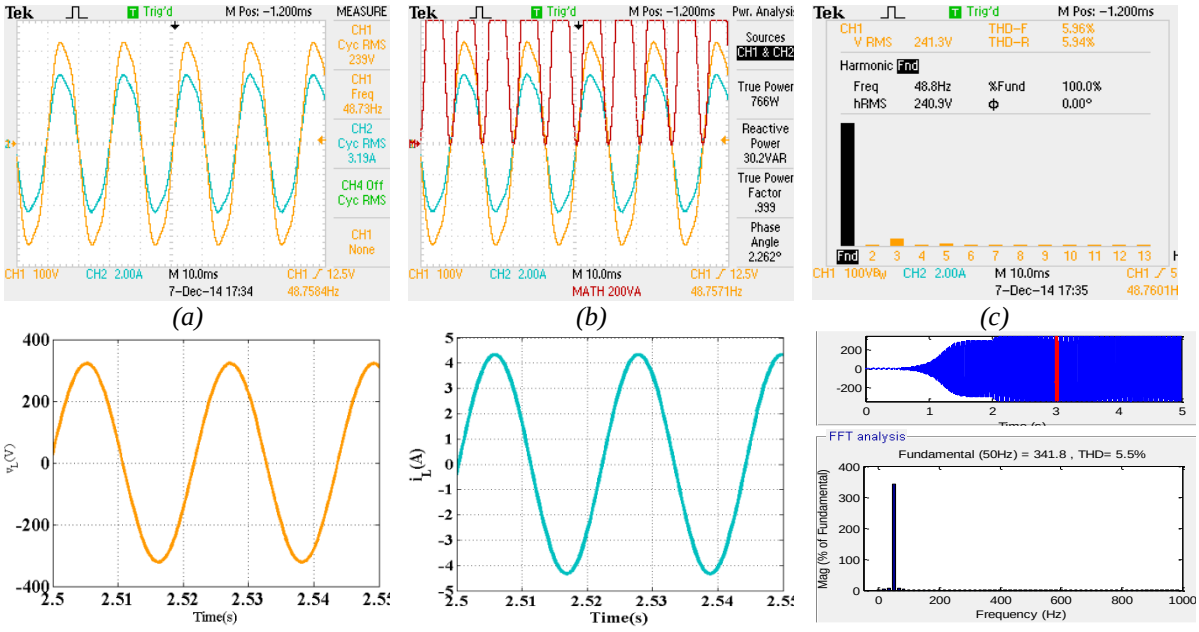

(a) (b) (c)

(d) (e) (f)

Figure 12. Recorded and simulated parameters of phase A at series capacitance of 40 µF at unity pf (a) load voltage and current (b) true and reactive powers along with operational pf (c) load voltage harmonics (d), (e) and (f) show the load voltage, current and load voltage harmonics respectively.

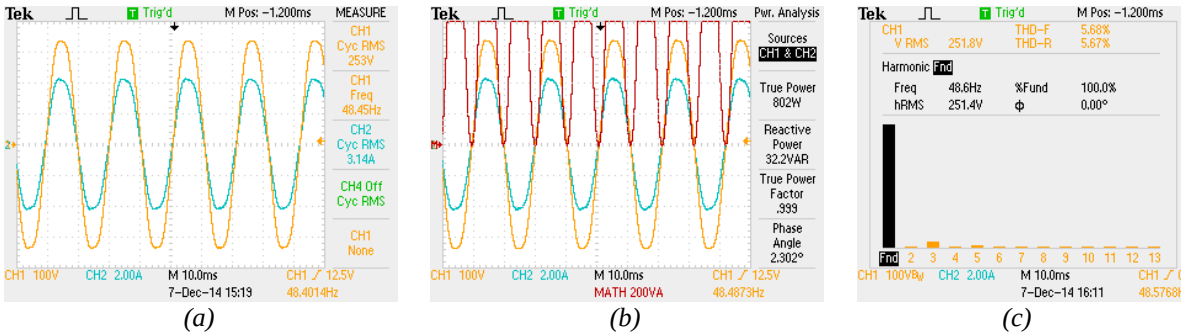

(a) (b) (c)

Figure 13. Recorded parameters of phase A at series capacitance of 50 µF at unity pf (a) load voltage and current (b) true and reactive powers along with operational pf (c) load voltage harmonics.

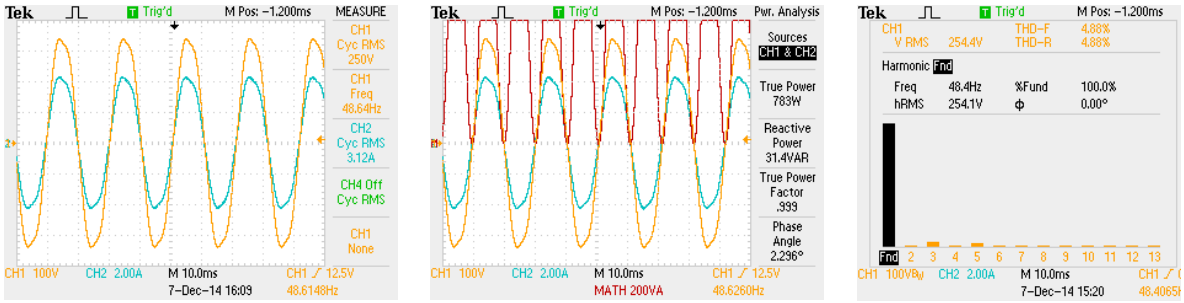

(a) *(b)* *(c)*

Figure 14. Recorded parameters of phase A at series capacitance of 70 µF at unity pf (a) load voltage and current (b) true and reactive powers along with operational pf (c) load voltage harmonics.

The phase *A* parameters of SEIG corresponding to the loading up-to rated value of 2.2 kW at unity pf for different excitation capacitances are tabulated in Table 1. The variations of load voltage (V_L) and output power (P_o) with respect to the C_{se} are also plotted in Fig. 15. Both the V_L and the P_o clearly demonstrate the identical behavior.

Table 1. Measured parameters of SEIG at different series capacitances with C_{ex}=15 µF and rated speed of 1500 rpm.

$C_{se}(\mu F)$	$V_L(V)$	$P_O(W)$	$I_L(A)$	THD(%f)
30	199	596	3.01	9.42
40	239	766	3.19	5.96
50	253	802	3.14	5.68
70	250	783	3.12	4.88

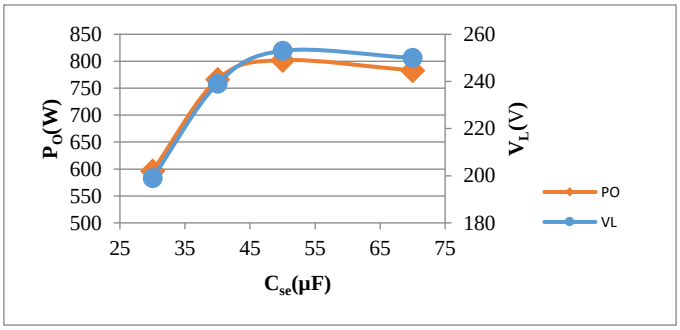

Figure 15. Variation of full-load voltage and output power of phase A of SEIG with different series capacitances at optimum excitation capacitance of 15µF and rated speed of 1500 rpm.

5.1.3. SEIG supplying *R-L* load

Retaining the same set of optimum capacitances the rated load of 0.9 lagging power factor is switched to the SEIG terminals with R_L=76 Ω and L_L=117 mH. The 0.9 power factor rated load is arranged through combination of variable R and L loads used for the analysis. The results are depicted in Fig. 16. Now, the interesting observation to be made here is that the full load voltage in the present case is more than that obtained for the unity power factor case. As can be seen from Fig. 16(d) the full load simulated voltage is about 382.3 V(279 V, rms). From the measured result the load voltage 381.8 V (270 V, rms). The variation in load current is less pronounced between the unity and 0.9 lagging pf as the load voltage has increased by about 40 V compared to unity pf case. The recorded and simulated currents are respectively 3.2 A and 3.13 A (rms) respectively. The reactive power drawn by the load shows the effect of power factor as it has increased in comparison to the unity power factor case earlier. For the unity power factor load the drawn reactive power is about 30.2 var/phase, whereas for 0.9 lagging power

factor it comes out to be 298 var i.e. more than 9 fold increase. The THDs of full load recorded and simulated voltages in the present case are illustrated by Fig. 16(c) and Fig. 16(f) respectively.

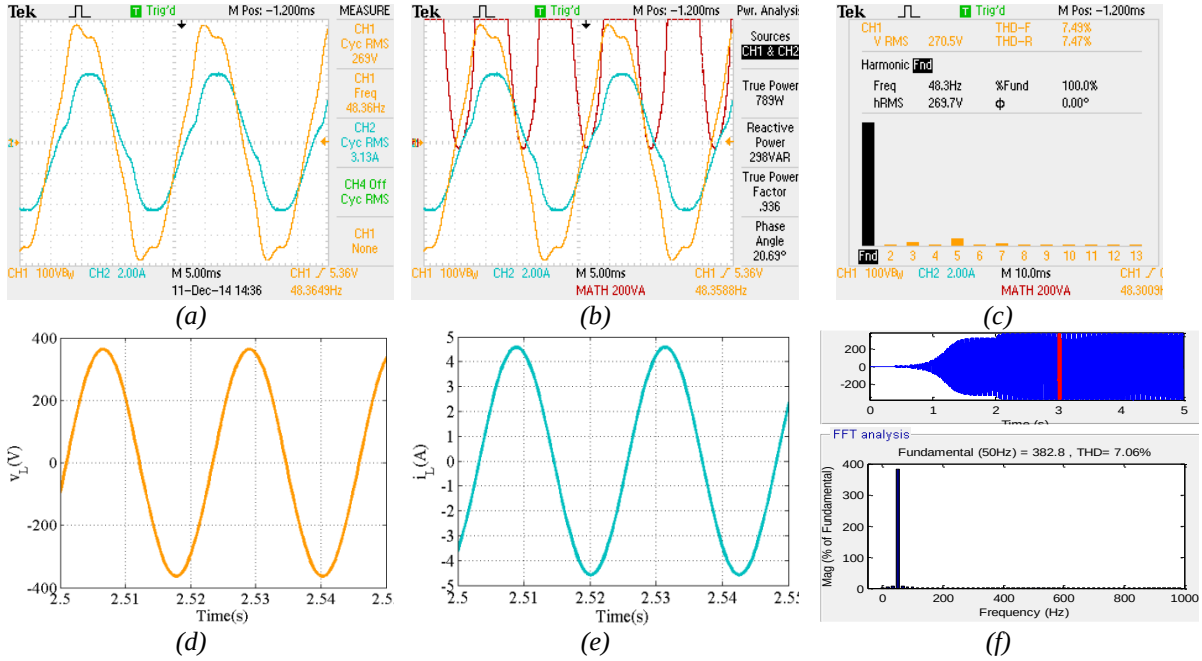

Figure 16.Recorded and simulated parameters of phase A with C_{ex}=15 μF and C_{se}= 40 μF at rated speed of 1500 rpm supplying rated load of 0.9 lagging pf (a) load voltage and current (b) active and reactive powers along with the operational pf (c) load voltage harmonics (d), (e) and (f) show the simulated load voltage, current and load voltage harmonics respectively.

Variation of different output parameters before and after 0.9 lagging power factor loading on the SEIG terminals is given in Fig. 17. It can be seen that as the load is switched on at t=2s the rms voltages and currents change in response. It is also observed that the response of terminal voltage V_T is identical to load voltage. This is attributed to the increase in current causing higher voltage drop and decreased voltage across the terminals. In the present case the change in magnetizing current can be observed as the load voltage has changed considerably. As can be seen from the curve depicting response of L_m, as soon as the loading is done the its value decreases to 0.78 from 0.84 on no-load as the load voltage settles down to its steady state at new operating point of 279 V (rms). The simulated active output power generated is 2270 W about 2% more than the measured results. The electromagnetic torque generated by the SEIG for the loading is around 25.6 Nm. The terminal voltage and stator current are respectively 262 V and 4.2 A. The magnetizing current of builds up to 4.2 A after the loading is affected. Simulated and experimental parameters for 0.9 lagging pf load are tabulated in Table 2.

Table 2 Simulated and experimental output parameters of SEIG supplying full loads (2.2 kW) at unity and 0.9 lagging pf.

	V_L(V), rms		***P_o(W)***		***I_L(A), rms***		**THD(%f)**	
pf	Exp'l	Sim'l	Exp'l	Sim'l	Exp'l	Sim'l	Exp'l	Sim'l
unity	239	241	766	741	3.19	3.1	5.96	5.5
0.9 (lag)	269	274	789	814	3.13	3.2	7.49	7.06

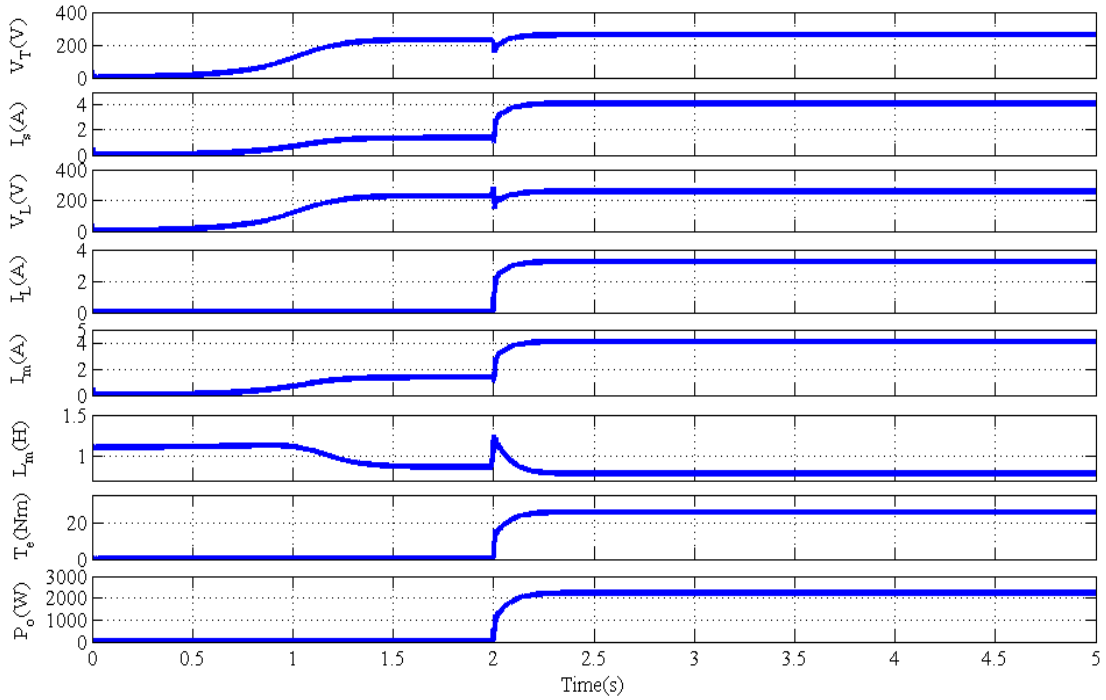

Figure 17. Variation of different SEIG parameters at full load of 0.9 lagging power factor

6. CONCLUSION

In this paper a detailed study of all the aspects associated with the mathematical modeling, Simulink implementation and the establishment of test-rig for a three phase, self-voltage regulating SEIG are reported. The step by step approach adopted for the d-q modeling of SEIG in stationary reference frame provides insights in-to various aspects related to self-excitation and voltage build-up. The parameters responsible for initiation of self-excitation from rotor side as well as the stator side are exclusively highlighted in the modeling. The developed simulation model of SEIG is included in the paper with details of each block provided in legible and easily comprehendible manner. Details of setting up a test-rig for three phase SEIG along with description of all the equipment and components employed are provided for easy reference. The importance of magnetizing inductance, L_m and its inclusion in the modeling through magnetizing characteristic are explained. Magnetizing characteristic is essential for the analytical study of SEIGs and it can be extraction through synchronous speed test of the induction machine. Procedure for performing synchronous speed test is explained and the obtained magnetizing characteristic of investigated machine is reported. Experimental selection of excitation and compensation capacitances is explained on the basis of relevant results. For the investigated machine the optimum excitation capacitance comes out to be 15 µF and the series capacitance as 40 µF. The SEIG is further operated with optimum capacitances to evaluate its characteristics for unity and 0.9 lagging pf. The results obtained for different loads are compared amongst them as well as with their corresponding measured results. Good agreement is achieved between the simulated and measured results. To conclude the analysis various operating parameters of SEIG supplying rated load of 0.9 lagging pf are analyzed.

REFERENCES

[1] Seyoum, D, Grantham, C, Rahman, MF. The dynamic characteristics of an isolated self-excited induction generator driven by a wind turbine. *IEEE Transactions on Industry Applications* 2003; *39*: 936-944.

[2] Palle, B, Somoes, MG, Farret, FA. Dynamic simulation and analysis of parallel self-excited induction generator for island wind farm systems. *IEEE Trans. on Industry Applications* 2005; *41*(4): 1099-1106.
[3] Haque, MH. A novel method of evaluating performance characteristics of a self-excited induction generator. *IEEE Transactions on Energy Conversion*2009;*24*(2): 358-365.
[4] Bašic, M, Vukadinovic´, D, Petrovic, G. Dynamic and pole zero analysis of self-excited induction generator using a novel model with iron losses. *International Journal of Electrical Power & Energy Systems* 2012; *42*(1): 105-118.
[5] Khan, MF, Khan, MR. Analysis of voltage buildup and speed disturbance ride-through capability of a self-excited induction generator for renewable energy application. *International Journal of Power and Energy Conversion* 2016; *7*(2): 157-177.
[6] Iyer, KLV, Xiaomin, Lu, Usama, Y, Ramakrishnan, V, Kar, NC. A twofold daubechies-wavelet-based module for fault detection and voltage regulation in seigs for distributed wind power generation. *IEEE Transactions on Industrial Electronics*2013;*60*(4): 1638-1651.
[7] Singh, B, Murthy, SS, Chilipi, RSR. Statcom-based controller for a three-phase seig feeding single-phase loads. *IEEE Transactions on Energy Conversion* 2014; *29*: 320-331.
[8] Chilipi, RR, Singh, B, Murthy, SS, Performance of a self-excited induction generator with dstatcom-dtc drive-based voltage and frequency controller. *IEEE Transactions on Energy Conversion* 2014; *29*(3): 545-557.
[9] Li, W, Dong-Jing, L. Coordination control of an ac-to-dc converter and a switched excitation capacitor bank for an autonomous self-excited induction generator in renewable-energy systems. *IEEE Transactions on Industry Applications* 2014; *50*(4): 2828-2836.
[10] Kumar, S, Kumaresan, N M, Subbiah, M, Rageeru, M. Modeling, analysis and control of stand-alone self-excited induction generator-pulse width modulation rectifier systems feeding constant DC voltage applications. *IET Generation, Transmission & Distribution* 2014; *8*(6): 1140-1155.
[11] Chauhan, PJJ, Chatterjee, K, Bhere, H, Perumal, BV, Sarkar, D. Synchronized operation of dsp-based generalized impedance controller with variable-speed isolated seig for novel voltage and frequency control. *IEEE Transactions on Industry Applications*2015;*51*(2): 1845-1854.
[12] Chan, TF. Performance analysis of a three-phase induction generator self-excited with a single capacitance.*IEEE Transactions on Energy Conversion* 1999;*14*: 894-900.
[13] Chan, TF, Lai, LL. A novel excitation scheme for a stand-alone three-phase induction generator supplying single-phase loads. *IEEE Transactions on Energy Conversion* 2004; *19*: 136-143.
[14] Singh, B, Singh, M, Tandon, AK. Transient performance of series-compensated three-phase self-excited induction generator feeding dynamic loads. *IEEE Transactions on Industry Applications* 2010: *46*(4): 1271-1280.
[15] Geng, H, Xu, D, Wu, B, Huang, W. Direct voltage control for a stand-alone wind-driven self-excited induction generator with improved power quality. *IEEE Transactions on Power Electronics*2011;*26*(8): 2358-2368.
[16] Mahato, SN, Singh, SP, Sharma, MP. Dynamic behavior of a single-phase self-excited induction generator using a three-phase machine feeding single-phase dynamic load. *Electrical Power and Energy System* 2013; *27*:1-12.
[17] Khan, MF, Khan, MR. Study on different loading topologies of a six-phase self-excited induction generator. *Engineering Science and Technology, an International Journal*2018; *21*(4): 654-663.
[18] Khan, MF, Khan, MR. Generalized model for investigating the attributes of a six-phase self-excited induction generator over a three-phase variant. *International Transactions on Electrical Energy Systems* 2018;*28*(10)*:* e2600.
[19] Khan, MF, Khan, MR. Modeling and Analysis of a Six-Phase Self Excited Induction Generator Feeding Induction Motors. *IEEE Transactions on Energy Conversion* 2020; *36*(2): 746-754.
[20] Thomsen, B, Guerrero, JM, Thogersen, PB. Faroe Islands wind-powered space heating microgrid using self-excited 220-kw induction generator. *IEEE transactions on sustainable energy* 2014;*5*(4): 1361-1366.
[21] Khan, MF, Modeling and control of multi-phase induction generator for wind energy applications. Ph.D. Dissertation. Aligarh Muslim University India, 2015.
[22] Khan, MF, Khan, MR. Comprehensive analytical and experimental analysis of a self-excited induction generator for renewable energy application. *International Journal of Renewable Energy Research* 2015; *5*(3): 746–756.
[23] Chauhan, YK, Yadav, VK, Singh, B. Optimum utilisation of self-excited induction generator. *IET Electric Power Applications*2013; *7*(9): 680-692.
[24] Lopes, LAC, Almeida, RG. Wind-driven self-excited induction generator with voltage and frequency regulated by a reduced-rating voltage source inverter. *IEEE Transactions on Energy Conversion* 2006; *21*(2): 297-304.

[25] Hilloowala, RM, Sharaf, AM. A rule-based fuzzy logic controller for a PWM inverter in a stand alone wind energy conversion scheme. *IEEE Transactions on Industry Applications*1996;*32*(1): 57-65.
[26] Simoes, MG, Bose, BK, Spiegel, RJ. Fuzzy logic based intelligent control of a variable speed cage machine wind generation system. *IEEE Transactions on Power Electronics* 1997;*12*(1): 87-95.
[27] Simoes, MG, Bose, BK, Spiegel, RJ. Design and performance evaluation of a fuzzy-logic based variable-speed wind generation system. *IEEE Transactions on Industry Applications* 1997;*33*(4): 956-965.
[28] Ahmed, T, Noro, O, Hiraki, E, Nakaoka, M. Terminal voltage regulation characteristics by static var compensator for a three phase self-excited induction generator. *IEEE Transactions on Industry Applications* 2004; *40*(4): 978-988.
[29] Chauhan, YK, Jain, SK, Singh, B. A prospective on voltage regulation of self-excited induction generators for industry applications.*IEEE Transactions on Industry Applications* 2010;*46*(2): 720-730.
[30] Khan, M F, Khan, M.R. December. Self-regulating three phase-self excited induction generator for standalone generation. In: 2013 Annual IEEE India Conference (INDICON), 13-15 Dec. 2013, IEEE Xplore, pp. 1-6.
[31] Khan, MR, Khan, MF. Dynamic Modeling and Analysis of a Self-Voltage Regulating Three Phase Self-Excited Induction Generator. *International Journal of Engineering Research in Electrical and Electronic Engineering* 2017; *3*(11): 14-19.
[32] Shrestha, GB, Haque, MH. AC circuits and Machines. Singapore: Prentice-Hall, 2006.
[33] Kalamen, L, Rafajdus, P, Sekerák, P, Hrabovcová, V. A novel method of magnetizing inductance investigation of self-excited induction generator. *IEEE Transactions on Magnetics* 2012; *48*(4): 1657-1660.
[34] Chan, TF. Steady-state analysis of self-excited induction generators. *IEEE Transactions on Energy Conversion*1994;*9*(2)*:* 288-295.
[35] Khan, M. F, Khan , MR, Iqbal, A. Effects of induction machine parameters on its performance as a standalone self-excited induction generator. *Energy Reports* 2022; *8*(2022): 2302-2313.

Appendix

EVALUATION OF MAGNETIZING CHARACTERISTIC:

Magnetizing characteristic of SEIG for this study is evaluated by performing synchronous speed test on induction machine employed as SEIG. To perform this test the stator windings of induction machine operated as SEIG are fed 3-phase voltages from a variable voltage as it is run from a prime mover maintaining rated speed of 1500 rpm. Direction of rotor movement and the revolving field of three-phase supply must carry same direction or else the field shall to avoid create braking effect.

To collect required data the supply voltage is varied in suitable steps starting from 0 to about 120% of its nominal value. At each step the per-phase applied voltage (V_{ph}) and the current as well as power drawn by the machine are noted. The magnetizing inductance L_m for each set of reading can be calculated from the available expressions [9].

Afterwards, variation between L_m and V_{ph} is formulated by fitting the data using "Basic Fitting" option of Matlab and the best fitting function yields the magnetizing characteristic.